Spatiotemporal variability of extreme precipitation in East of northwest China and associated large-scale circulation factors

Yuhong Guo (gyh1982@outlook.com)
Zaozhuang University https://orcid.org/0000-0001-9589-1747
Xiaodong Yan
Beijing Normal University https://orcid.org/0000-0002-0774-9140
Zhibo Gao
Beijing Normal University
Shuaifeng Song
Beijing Normal University

Research Article

Keywords: ENW, EPIs, spatiotemporal characteristics, trend, large-scale circulation factors

Posted Date: May 17th, 2023

DOI: https://doi.org/10.21203/rs.3.rs-2667499/v1

Spatiotemporal variability of extreme precipitation in East of northwest China and associated large-scale circulation factors

Yuhong Guo[a, b], Xiaodong Yan[b, *], Zhibo Gao[b], Shuaifeng Song[b]

a College of Tourism, Resource and Environment, Zaozhuang University, Zaozhuang, 277160, China
b State Key Laboratory of Earth Surface Processes and Resource Ecology, Beijing Normal University, Beijing, 100875, China
* Corresponding author, Email: yxd@bnu.edu.cn

Abstract

Spatial and temporal distributions and influencing factors of extreme precipitation are important bases for coping with future climate change. The spatiotemporal variability and affecting factors of extreme precipitation indices (EPIs) in East of northwest China (ENW) during 1961-2015 were investigated using a series of approaches such as modified Mann-Kendall trend test, Hurst exponent, Ensemble empirical mode decomposition (EEMD), and geodetector model. The results showed that CDD and CWD decreased significantly ($P<0.01$), with rates of 1.4 days/decade and 0.07 days/decade, respectively. EPIs in ENW exhibited an obvious heterogeneity. CDD gradually increased from the southeast to the northwest. The remaining EPIs generally showed the opposite trend. Some stations in ENW may experience more extreme precipitation events in the future. Geodetector results demonstrated that large-scale circulation factors had a significant impact on EPIs in ENW. The influence of large-scale climate factors on EPIs was concentrated in nonlinear enhancement, and Nino3.4 and SO were the dominant driving factors that played a major role in the variability of EPIs. The results of this study provided a reference for ENW and other arid and semi-arid regions to cope with extreme climates and develop corresponding strategies.

Keywords: ENW, EPIs, spatiotemporal characteristics, trend, large-scale circulation factors

1 Introduction

Climate change has been an indisputable fact (IPCC, 2013). It could lead to a series of catastrophic consequences in ecosystems, agriculture, and human health (WMO, 2021). Moreover, climate change profoundly affects the frequency and intensity of extreme climate events (Ahsan et al. 2022; Gudmundsson et al. 2021; Rafatnejad et al. 2022). In recent years, heat, flood, and drought records have been repeatedly broken in several countries (Rastogi et al. 2020; Schiermeier, 2021). Numerous rare extreme heat wave events have been reported in China, the United States, and most European countries over the past few years (Kendon et al. 2021; Lhotka and Kyselý, 2022; Lu et al. 2023; Marengo et al. 2022). Since June, July, and August 2022, there had been numerous widespread, long-lasting, polarized, and high-impact regional heat processes across much of China (Lu et al. 2023). More alarmingly, the heat wave continued in much of southern China until mid-September. In addition, severe droughts, which are a common accompaniment to heat waves, hit southern China. Persistent high temperatures and droughts would have caused power shortages, reduced crop yields, and heat exhaustion in many parts of China.

In addition to direct losses, extreme weather events such as torrential rains, high temperatures, heat waves, and droughts can trigger wildfires, flash floods, and mudslides, further exacerbating economic losses and societal casualties. As a result, scientists all around the world have launched comprehensive research on global climate change and extreme events (Descals et al. 2022; Donat et al. 2016; Fischer and Knutti, 2015; Kirschbaum et al. 2020). So far, climate scientists now agree that carbon emissions from human burning of fossil fuels are warming the planet, aggravating the risk and severity of droughts, heat waves, and other extreme weather events (Perkins-Kirkpatrick et al. 2022; Sun et al. 2021; Yang et al. 2022).

Extreme weather events are influenced by many conditions (Ali et al. 2018; Berg et al. 2009; Li et al. 2020). Among them, large-scale circulation is considered one of the most important factors (Das, 2021; Zhang et al. 2021). Sun and Zhang (2017) found that the Northwest Pacific Subtropical High (WNPSH) affects extreme precipitation by triggering changes in tropical cyclones, and its intensity and location are closely related to precipitation in southern China. Liu et al. (2021) demonstrated that the positive Pacific meridional mode (PMM) phase is accompanied by suppression of extreme precipitation in the middle and lower reaches of the Yangtze River (MLYRB) and enhancement of extreme precipitation in North China (NC). ENSO has a significant impact on extreme precipitation events around the world (Wang et al. 2014). In the Gulf Coast (GC), East Coast (EC), and SW (Southwest Coast) of the United States, extreme storms (one-in-20-year storms), which occur on average only once every 20 years, occur on average half the time under persistent El Niño conditions (Schubert et al. 2008). Zhang et al. (2020) reported that the combination of a positive PDO (+PDO) and a negative AMO (-AMO) changing to a negative PDO (-PDO) and a positive AMO (+AMO) has a great impact on the interdecadal shift in extreme high temperature in North China in 1996. In addition, PDO and AMO also have an important impact on the impact of ENSO on extreme climate events. When in phase with PDO, dry-wet changes induced by ENSO are amplified relative to the standard model. Wang et al. (2014) concluded that the effect of ENSO on wet-dry changes varied with the PDO stage.

China has a large area and a multiplicity of terrain, which leads to a complex and diverse climate, including both monsoon and non-monsoon climate types, and obvious heterogeneity of precipitation. The complex climate has made China one of the countries severely affected by meteorological disasters. In the context of global climate change, the frequency of extreme weather events with extreme weather and climate events with great destructive influence in China has also increased significantly, such as heat waves, cold waves, heavy rains and severe droughts, sandstorms, floods, and compound extreme climate events (Liao et al. 2021; Yin et al. 2022; Zhou et al. 2022). The above phenomena are also consistent with previous research results. For example, Liu et al. (2015) reported that although total precipitation in rural and urban meteorological stations in eastern China does not change much, light precipitation decreases significantly, and heavy precipitation increases significantly. Average annual precipitation in southwest, northwest, and east China increased significantly, and annual precipitation in central, northern, and northeastern regions decreased significantly (Wang and Zhou 2005). In addition, rising trends in the fractional contribution of hot weather to extreme precipitation events over most parts of China have accelerated in more recent decades (Ning et al. 2022).

Northwest China has a complex topography, belongs to arid and semi-arid climate zones, and the temporal and spatial distribution of precipitation is uneven. Therefore, when studying the northwest region, it is often divided into east and west separately from the perspective of climate. The eastern part of Northwest China is adjacent to Northeast China and North China, so the study of changes in the extreme precipitation index is of great significance to local agriculture and ecosystems. Previous studies have shown that precipitation days in the eastern part of the Northwest Territories have shown a decreasing trend over the past half century (Chen and Dai, 2009; Wang et al. 2021; Yao et al. 2017). However, until now, few scholars have analyzed the precipitation variation characteristics of ENW from the perspective of EPIs. Therefore, this study calculated the 10 EPIs in ENW recommended by the World Meteorological Organization (WMO)'s Expert Team on Climate Change Detection and Indices (ETCCDI), and analyzed their change characteristics, trends, and possible influencing factors, in order to provide a basis for local agricultural production and meteorological disaster prevention and better design of local climate change adaptation strategies.

2 Study area

With reference to Mao et al. (2010), China was divided into eight subregions, according to the geographical area and monsoon specificity. East of northwest China (35.25-42.75°N, 97.25-110.25°E) was chosen as the study area in this study (Fig. 1).

Located on the northeastern side of the Qinghai-Tibet Plateau, the whole region of northwest China has vast and complex terrain, which is a sensitive area to climate change. The study area is East of northwest China including most of Gansu, northeastern Qinghai, all of Ningxia, western Inner Mongolia, and northern Shaanxi. The terrain mainly consists of the plateau and flat land. It is an arid and semi-arid region, and the water vapor conditions inside the region are poor, where water vapor formation mainly depends on transport outside the region (Zhu et al. 2013). Stations are evenly distributed except for areas such as deserts.

3 Data Source And Methodology

3.1 Data source

In this study, the daily precipitation data of 63 meteorological stations in the eastern part of northwest China from 1961 to 2015 were selected from the daily dataset of ground climate data in China (Dataset V3.0), which is a common data source in remote sensing, GIS, hydrology, climate change, and other research fields (http://data.cma.cn/) (Guo et al. 2019; Liu et al. 2019; Qian, 2016). Dataset V3.0 contains 699 benchmarks and basic weather stations in China. Since many stations were not established before 1961, the data start time for this study is 1961. A small amount of missing data in individual stations was completed by forward and backward interpolation methods to ensure data continuity. Meanwhile, some stations with very short period of data or more than 5% of missing data were deprecated. The spatial location of these 63 meteorological stations is shown in Fig. 1 and their attributes are shown in Table 1.

The atmospheric circulation indices were downloaded from the National Oceanic and Atmospheric Administration of the United States (https://www.noaa.gov/), including the Pacific Decadal Oscillation (PDO), Tripolar Index for the Interdecadal Pacific Oscillation (IPO), Arctic Oscillation (AO), North Atlantic Oscillation (NAO), Atlantic Multidecadal oscillation (AMO), Nino3.4 and Southern Oscillation (SO).

3.2 EPIs selection

The ETCCDI first developed and recommended 27 extreme climate indices for the objective measurement and characterization of temperature and rainfall variability and change. In this study, a total of 10 precipitation-related climate indices were calculated and analyzed for a better understanding of historical change characteristics (Table 2).

3.3 Methodology

3.3.1 Modified Mann-Kendall trend test

A Mann-Kendall trend test (sometimes called the MK test) is a non-parametric method and can be applied to all distributions (i.e. the data do not have to satisfy the assumption of normality). It has been widely used as a statistical technique in analyzing the increasing or decreasing trend of time series data (Kendall, 1957; Mann, 1945). In addition, the advantage of the MK test is that it is not affected by missing data or outliers, which are common in meteorological data. The modified Mann-Kendall test was used to analyze consistently increasing or decreasing trends (monotonic trends) of EPIs in this study, which has the ability to eliminate the influence of serial correlation on the MK test (Yue and Wang, 2004).

3.3.2 EEMD

The EEMD method is an improved version of empirical mode decomposition (Wu and Huang, 2009). It is based on the principle of multiple averaged measurements, by adding different series of white noise into the signal in the original observation data to overcome modal aliasing (Qian et al. 2011). It is a powerful tool for denoising variable signals and is suitable for analyzing non-linear and/or non-stationary time series.

3.3.3 R/S method for calculating Hurst index

Hurst exponent was originally established by the famous hydrologist Harold Edwin Hurst to quantify the relative trend in the time series of reservoir storage capacity (Hurst, 1951). It is a judgment index and is widely applied to other natural systems to measure the long-term memory of time series, such as finance, meteorology, remote sensing, and other fields (Onali and Goddard, 2011; Rivas-Tabares et al. 2021). In this study, the rescaled range R/S method was adopted to calculate the Hurst index of different extreme precipitation indicators at each station.

Suppose there is a time series named $\xi(t)$, and $t = 1, 2, 3, \ldots$ .For any positive integer $\tau \geq 1$, a mean sequence is as follows:

$$\langle\xi\rangle_\tau = \frac{1}{\tau}\sum_{t=1}^{\tau}\xi(t)\,\tau, \tau = 1, 2, \ldots. \tag{1}$$

Cumulative deviation could be calculated as follows:

$$X(t,\tau) = \sum_{\mu=1}^{t}(\xi(\mu) - \langle\xi\rangle_\tau)\ , 1 \leq t \leq \tau. \tag{2}$$

The range could be calculated as follows:

$$R(\tau) = \max_{1\leq t\leq\tau} X(t,\tau) - \min_{1\leq t\leq\tau}(t,\tau),\ \tau = 1, 2, \ldots \tag{3}$$

The standard deviation could be calculated as follows:

$$S(\tau) = \left[\frac{1}{\tau}\sum_{t=1}^{\tau}(\xi(t) - \langle\xi\rangle_\tau)^2\right]^{\frac{1}{2}} \tag{4}$$

The ratio of range to standard deviation could be calculated as follows:

$$R(\tau)/S(\tau) \triangleq R/S. \tag{5}$$

After long-term theoretical analysis and simulation test research, Hurst found the following empirical scaling relationship:

$$R(\tau)/S(\tau) = (\frac{\tau}{2})^H. \tag{6}$$

Where H is the Hurst exponent and could be calculated.

The trend could be judged by Hurst Value. A Hurst index between 0.5 and 1 suggests that the returns are persistent. At 0.5, the index suggests returns are completely random. Between 0 and 0.5, it suggests that the returns are mean reverting.

3.3.4 Geodetector Model

The Geodetector Model, also known as a geographical detector, consists of a series of statistical tools for measuring spatial stratified heterogeneity (SSH) and attribution for/by SSH (Wang et al. 2016), which refers to phenomena within strata that are more similar than that between strata. This method has been widely used in various fields such as ecology, medicine, and meteorology (Li et al. 2017; Li et al. 2020; Yin et al. 2019). In this study, the factor detector was used to discover large-scale climatic teleconnections factors.

The contributions of factors (q value) can be calculated by the following formula:

$$q = 1 - \frac{\sum_{h=1}^{L} N_h\sigma_h^2}{N\sigma^2}\ \text{, and } q \in [0,1]. \tag{7}$$

Where N and s^2 stand for the number of units and the variance of Y in a study area, respectively; the population Y is composed of L strata (h = 1, 2, …, L); N_h is the layer h in the whole study area; σ_h^2 is variances of the dependent variables within the whole area and layer h, respectively. The value of q corresponds to the degree of contribution of each influencing factor to the dependent variable. Before reading data in Geodetector software, the explanatory variables must be a certain category of quantity through the natural break point classification.

Meanwhile, the interaction detector was used to determine the effects of interactions between large-scale teleconnection factors on EPIs. The interaction results in Table 3 represent the interaction relationship between the two factors. It has 5 intervals (Table 3) and the interaction relationship is determined by the location of $q(x \cap y)$ in the 5 intervals.

4 Results

In this study, extreme climate indices in ENW over the 1961-2015 period were calculated. 10 EPIs were selected for variations in spatial and temporal characteristics, which exhibited the frequency and intensity of rainfall characteristics.

4.1 Temporal variations of EPIs

We calculated all EPIs for each station and derived the annual regional EPIs in the study area. The interdecadal trends of each extreme precipitation index were fitted with a low-pass filter and their general trend lines were plotted (Fig. 2). Overall, CDD and CWD decreased significantly ($P<0.01$) at 1.42 days/decade and 0.07 days/decade, respectively. R95p and RX5day decreased non-significantly at 0.66 mm/decade and 0.01 mm/decade, while PRCPTOT, R10, R20, R25, R99p, and RX1day increased at a non-significant rate (Table 4). The mean values of CDD and CWD were 99.34 and 4.13 days, respectively. There was a significant synchronization between peak and trough values for both CDD and CWD metrics, and the overall trend for both was a considerable decrease. Although the low-pass filtered results of CDD showed a significant downward movement of the peak at a time than at a place, the low-pass filtered results of CWD displayed a rebound after the wave peak decreased. The distribution of PRCPTOT ranged from 210.00 mm to 406.84 mm, and the very low value represented a severe drought in the region during that year. The distribution characteristics of PRCPTOT and R10 in both raw data and low-pass filter results and trend lines were highly similar. From the changes in the two low-pass filter indicators, both were slowly decreasing and then rebounding, and the rebounding time occurred after 1990.

Similarly, R20 and R25 have extremely similar time-varying characteristics, both slowly decreasing and then slowly rebounding, but the turning point for their rebound occurred in 1982. R95p, R99p RX1day, and RX5day had similar time-varying characteristics and general trends. Unlike the other indicators, these four indicators tended to had a clear downward trend after a slow rebound, and the last decline was in 2010. The overall change results of the above indicators demonstrated that the change rates of the extreme precipitation indicators were not consistent. Combining the time series characteristics and change trends of all indicators, it can be found that although the frequency and intensity of ENW extreme precipitation events moderated in the 1980s and 1990s and began to intensify around 2010, the peaks of PRCPTOT, R10, R20, and R25 around 1990 were significantly lower than those in the 1960s. After 2000, R99p and RX1day had higher peaks than all previous years, indicating an increase in the intensity of the overall short-duration intense precipitation in the region. Thus, although the overall aridity of the ENW decreased (CDD declined), the overall trend towards wetness was not significant (CWD also declined significantly but by a smaller absolute amount). The above data indicated that the overall decrease in the frequency and intensity of extreme precipitation in the region over the past few years has tended to increase again, so it is highly likely that extreme precipitation events of this tendency will change from insignificant to significant in the future.

In addition to the general trend of increasing and decreasing over time, each extreme climate index exhibited a certain periodicity. The periods of all EPIs were calculated using the EEMD method to further explore its temporal variation pattern (Fig. 3). The cycles of Period 1 and Period 2 range from 1.53 to 3.06 years and 2.29 to 4.58 years, respectively, reflecting the quasi-2-year and 4-5-year oscillations of the above indices. In addition, low-pass filtered results of CDD and CWD indicated an interdecadal variation cycle from 1961 to 1990 and 1990 to 2015, respectively. Interdecadal cycles of PRCPTOT, R10, R20, and R25. On the other hand, with a range of 10 to 20 years. R95p, R99p, RX1day, and RX5day had similar characteristics of interdecadal variation. The above indices had similar interdecadal periodicity. The periodic variations of the above indices are synchronized with the cycles of atmospheric circulation factors. The El Niño-Southern Oscillation (ENSO) phenomenon dominates climate fluctuations on interannual time scales, with periods ranging from 2 to 7 years

(Lu et al. 2018). AO has obvious major cycle changes of 2.6-2.9 years and 3.7 years and long-term oscillations of 9-26 years, and the oscillation cycle of IPO and PDO is 20-30 years. Therefore, the similarity of the above cycles initially indicated that various large-scale circulation factors may be related to EPIs.

4.2 Spatial Distribution of EPIs

Overall, the spatial distributions of all EPIs had both similar spatial distribution characteristics and some differences. CDD and CWD can reflect the degree of dry and wet weather in the study area, respectively. The spatial distribution of the two was highly regular (Fig. 4a and 4b). From 1961 to 2015, the CDD frequency range in ENW was 52.15-213.19 days. The lowest value of CDD occurred at the southernmost end of ENW, Luochuan in central Shaanxi; the highest value occurred at the northernmost end of the region (Ejina Banner, Inner Mongolia). Roughly speaking, the value of CDD increased from the southeast to the northwest (increasing along the direction of the vertical red and black arcs in Fig. 4a). CWD ranged from 1.69 to 7.84 days, with the lowest value of CWD still emerged in Ejina Banner, Inner Mongolia, while the highest value of CWD occurred in Yeniugou, Kangding County. The spatial distribution trend was just opposite to that of CDD, gradually decreasing from the southeast to the northwest.

The annual frequency of R10 ranged from 0.58 to 18.85 days, and its highest and lowest values appeared in Luochuan, Shaanxi, and Ejina Banner, Inner Mongolia, respectively, which was just opposite to the results of high and low CDD stations. The overall spatial pattern of R10 was similar to that of CWD, i.e. high values occurred in the south, low values appeared in the north, and gradually decreased from the southeast to the northwest. Similar to R10, the distribution trends of R20 and R25 were also high in the south and low in the north, but the distribution ranges were 0.09-8.05 days and 0.04-4.91 days respectively. In addition, the intensities of R20 and R25 were lower in the southwest corner of ENW, and their distributions had more obvious similarities.

The spatial distribution characteristics of PRCPTOT were similar to those of CWD, with absolute values ranging from 31.31 to 601.19 mm. In particular, PRCPTOT had low values in the northern part of ENW. The distribution of this index showed that the distribution of CWD and PRCPTOT had good synchronization.

R95p and R99p, which represent extreme precipitation intensity, can reflect the degree of humidity in the region, and R99p is more humid. The variation ranges of R95p and R99p were 7.20-151.64 mm and 2.21-59.49 mm, respectively. The spatial distributions of the two indices were also very similar, meaning the degree of humidity decreased rapidly from the southeast to the northwest, indicating that the northwest of the region is extremely dry.

RX1day and RX5day, which represent precipitation intensity, had extremely similar spatial distribution rules. The ranges of RX1day and RX5day were 10.45-60.21mm and 13.69-99.06 mm respectively, and the range of RX5day was about 1.5 times that of RX1day. The spatial distribution of RX1day and RX5day showed that the southeast had the highest rainfall, while the northwest had the lowest. That said, the risk of short-term heavy precipitation in the southeast was greater than that in the northwest. The highest and lowest stations of RX1day and RX5day were Ejina Banner in Inner Mongolia and Luochuan in Shaanxi, respectively. Based on the above, it can be found that the overall trend of ENW is gradually drying from the southeast to the northwest, and there was a huge difference between the northwest and the southeast. As a result, the northern part of this area was relatively dry and lacking precipitation, while the southern part was relatively rich in precipitation.

4.3 Future trends of the EPIs

In order to predict the spatial variation characteristics of each extreme precipitation index in ENW in the future, the R/S analysis method was utilized to calculate the Hurst index of all EPIs. Fig. 5 illustrated that the proportion of stations with Hurst values greater than 0.5 for each extreme precipitation index in ENW stations was relatively high. Among them, stations with Hurst values of R10 greater than 0.5 accounted for the highest proportion, reaching 71.43%. For the R95p index, the number of stations with Hurst >0.5 was the lowest at 55.56%. The data of the above ratios showed that the various EPIs of ENW in the future will mainly maintain the original trend. In terms of spatial distribution, stations with Hurst values <0.5 of CDD and CWD were mainly located in Gansu and Ningxia. The areas where PRCPTOT's Hurst value was less than 0.5 were concentrated in Baotou, Bayannur, Yinchuan, Ordos, and Wuhai. The stations with the opposite trend of R20 were mainly concentrated in Bayannaoer, Wuhai, Ordos, and Yulin. The remaining stations with Hurst values <0.5 in the future were mainly located in Inner Mongolia, Qinghai, and southern Gansu. The spatial distribution of the above-mentioned EPIs had very similar distribution characteristics, indicating that the overall trend of various extreme precipitation was basically the same in ENW, and the above-mentioned stations with Hurst < 0.5 are more sensitive to climate change and prone to reverse trends.

Using the modified MK test to detect the temporal change trend of each index at each station, and combining it with the Hurst index, the future change trends of all the stations in ENW were illustrated in Fig. 6. In the future, the CDD of 16 stations in ENW will show a significant upward trend, 16 stations will show a significant downward trend, and the rest will have no significant trend. That is to say, the drought degree of 25.40% of the total num of stations will ease in the future, and the frequency of persistent drought will increase significantly in 25.40% of the total number of stations in the future. In the future, the CWD of 12 stations will increase significantly, and that of 7 stations will decrease significantly, indicating that 19.05% of the total number of stations will become more humid in the future, while 11.11% of the total number of stations will become less humid in the future. In the future, R10 and R20 will increase significantly at 26.98% and 11.11% of the total number of stations. In contrast, R10 and R20 will decrease significantly at 20.63% and 9.52% of the total number of stations. These figures demonstrated that there would be more stations with increased heavy precipitation than decreased stations in the future. In PRCPTOT, 23 stations would undergo a significant increase, 20 stations would see a significant decrease, and the rest would have no significant trend. In the future, for R95p, R99p, RX1day, and RX5day, 17.46%, 17.46%, 23.81%, and 25.40% of the total number of stations will increase significantly, indicating that the intensity of extreme precipitation will increase in the future. 20.63%, 11.11%, 20.63%, and 17.46% of the total number of stations R95p, R99p, RX1day, and RX5day will decrease significantly, indicating that the intensity of extreme precipitation at these stations will decrease in the future. In conclusion, there would still be a substantial percentage of the total number of stations where the frequency and intensity of extreme precipitation increase significantly in the future. Stations with reduced intensity and frequency account for the least. Therefore, the challenges of future meteorological and water environment management will be even greater.

4.4 Contribution of large-scale teleconnections to extreme precipitation variability

As mentioned in the introduction, the frequency and intensity of extreme weather events are closely related to the large-scale circulation indices (Gao et al. 2017; Peng, 2018). ENW is a typical arid and semi-arid region. The relationship between the intensity and frequency of extreme precipitation in this region and large-scale teleconnection factors is of great significance for understanding the causes of precipitation changes in EPIs. Geodetector was adopted to explore the extent to which large-scale climatic teleconnections affect EPIs and the interaction of the above-mentioned impact factors.

The magnitude of the effect of each circulation factor on EPIs is identified by the *q* values, which is one kind of output in GDM. On the basis of the *q* statistics, the impact of each circulation index on the frequency and intensity of all EPIs were illustrated in Fig. 7(a) and Fig. 7(b). In general, EPIs were all affected by all these atmospheric circulation indices due to ocean-atmosphere interaction. Among the above factors, the large-scale factors that exerted the main influence on the frequency (CDD, CWD, R10, R20, and R25) of extreme precipitation were Nino3.4, SO, AO, and PDO. In contrast, the large-scale factors that had the greatest influence on the intensity (PRCPTOT, R95p, R99p, RX1day, and RX5day) of extreme precipitation were Nino3.4, SO, PDO, and AMO. Among the factors, the contribution ratios of Nino3.4 to CDD, CWD, R10, R20, and R25 were 13.80%, 10.16%, 15.07%, 16.15%, and 22.23%, respectively. The contribution percentages of Nino3.4 on PRCPTOT, R95p, R99p, RX1day and RX5day were 15.64%, 19.86%, 23.00%, 19.14% and 17.47%, respectively. The contribution ratios of SO to CDD, CWD, R10, R20, and R25 were 4.84%, 16.89%, 13.95%, 17.57%, and 24.23%, respectively. The contribution percentages of SO on PRCPTOT, R95p, R99p, RX1day and RX5day were 15.30%, 17.18%, 12.83%, 12.11% and 17.38%, respectively. Different EPIs responded differently to each atmospheric circulation factor. For instance, AO was the second largest driving factor to CDD, with a contribution of 11.62%. PDO was the second largest driving factor to CWD, with a contribution rate of 6.95%. Overall, Nino3.4 and SO were the main climatic drivers regulating precipitation frequency and intensity in ENW. There were differences in the response of each index to large-scale circulation factors.

EPIs are subjected to a combination of factors, and there are complex interactions between these factors. Therefore, it is necessary to quantify the interaction between the various atmospheric circulation factors. The results of the interaction of the various circulation factors were shown in Fig. 8. There are 5 intervals of interaction in the interaction factor detector, including "$(-\infty, \min(q(x), q(y)))$", "$(\min(q(x), q(y)), \max(q(x), q(y)))$", "$(\max(q(x), q(y)), q(x) + q(y))$", "$q(x) + q(y)$", "$(q(x) + q(y), +\infty)$". The interaction relationship is determined by the location of $q(x\cap y)$ in the 5 intervals (Table 3).

In this study, the interaction results of two driving factors on EPIs consist of two categories: nonlinear enhancement and bivariate enhancement. Therefore, the combined contribution of two factors to extreme precipitation events was larger than the contribution of individual factors. The interaction of two factors often had a greater effect on extreme precipitation than the sum of each factor and was often attributed to nonlinear enhancement. However, some exceptions existed in the following situations. For instance, Nino3.4∩SO exhibited bivariate enhancement for the indices of PRCPTOT, R10, R20, R25, R95p, R99p, and RX5day. PDO∩SO showed bivariate enhancement for R25. AO∩NAO manifested bivariate enhancement for the indices of R99p, RX1dayand RX5day. AO∩Nino3.4 revealed bivariate enhancement for RX1day. Nino3.4 and SO were both major contributors to the interaction results, which was consistent with the conclusion that Nino3.4 and SO were two of the most important factors in the univariate effects. In the majority of EPIs, most of the factors interacting with Nino3.4 and SO had greater explanatory power for EPIs. Taking CDD as an example, the explanatory power of AO was 11.62%. On contrary, the explanatory powers of AO∩Nino3.4 and AO∩SO reached 37.31% and 47.62%, respectively, indicating that the combined effect of Nino3.4 and SO can adequately affect the changes in CDD. IPOs and PDOs also strongly affect the interaction of some indicators, such as R99p, the interactions of IPO and AO had the strongest contribution to its changes.

5 Discussion

5.1 Spatiotemporal pattern and trend of EPIs

EPIs showed strong spatial and temporal variability in ENW. In terms of temporal variability, both CDD and CWD decreased significantly in ENW. Although EPIs have an overall upward or downward trend, they also exhibit certain cyclical patterns. For instance, cycles of 1-3 years and 3-5 years, and more than 10 years (Fig. 2).

The indices showed specific geographical patterns, with CDD increasing from the southeast to the northwest, while the spatial trends of the remaining indicators are opposite. At the same time, each index also exhibited obvious spatial heterogeneity. Since the climate of the region where each meteorological station is located is influenced by various factors such as geographical location, climate, and human activities, the spatial heterogeneity of meteorological element changes is prevalent, not only across regions significantly, but even between different sub-regions of the same region. Wang et al. (2022) found that regional spatial heterogeneity was also evident at Taihu Lake in the Yangtze River Delta, and that spatial heterogeneity of extreme precipitation was evident in China. Overall, total precipitation decreased in southwest and southern China, but extreme precipitation and intensity increased, making them prone to severe meteorological hazards. In contrast, EPIs will decrease in Northwest and North China. Extreme precipitation tends to increase in northern Xinjiang, China, while it tends to fall in other regions (Jiang et al. 2013). In Northeast China, frost day (FD0) decreased significantly, and SU25, TR20, and TX90 increased significantly, but the extreme precipitation index did not change significantly (Guo et al. 2019). The results of this study are constant with those of the above-mentioned studies in Northwest, Xinjiang, and Central Asia (Zhang et al. 2022).

We analyzed characteristics of the spatial and temporal distribution of each extreme precipitation index and the main circulation influences in ENW from 1961 to 2015. Although the average results for the whole region showed that only CDD and CWD had significant decreasing trends, and the increasing and decreasing trends of the remaining EPIs were not significant, a large percentage of stations showed significant increasing or decreasing trends. In particular, the Hurst index results combined with the improved MK test showed that for CDD, PRCPTOT, R10, and RX1day, 25.40%, 36.51%, 26.98%, and 23.81% of the total number of stations with significant increases in the future, respectively, indicating that about a quarter of ENW still experience an increase in both the frequency and intensity of heavy precipitation. Climate change plays an important role in the increase in extreme precipitation events. The combination of meteorological elements itself had some spatial and temporal heterogeneity, resulting in a decrease in both the intensity and frequency of extreme precipitation at a small number of NEW stations. Some studies pointed out that both precipitation and atmospheric water content in northwest China are increasing in the context of global warming (Zhang et al. 2020; Zhang and Zhou, 2019). And some soils in northwest China are dry and have poor soil and water conservation capacity. Extreme climatic events such as short-term heavy precipitation are prone to trigger disasters such as drought, flash floods, and mudslides (Wan et al. 2021). Therefore, the increasing trend of the above-mentioned extreme climatic events has seriously challenged local land resource management. For example, on August 17, 2020, an extraordinary rainstorm in Zhouqu County, Gansu Province, triggered severe mudslides and caused huge losses.

5.2 Possible driving factors of extreme precipitation variation

Our results provided obvious evidence that El Niño and SO were the most important factors influencing EPIs. Although each EPI was the result of a combination of factors, it showed bivariate and nonlinear enhancement in the contributions of all EPIs among the above drivers. But in all the final results, El Niño and Southern Oscillation (ENSO) were the main factors for the variation of all the EPIs. This was mainly because ENSO affected global temperature and precipitation through large-scale atmospheric and oceanic heat and moisture exchange. ENSO may lead to extreme precipitation events in Northwest China by affecting spring and summer precipitation in that region. This is due to the El Niño phenomenon that warms the Indian Ocean waters and thus raises the upper tropical potential height, which leads to the southward extension of high pressure in South Asia and further leads to positive pressure low-pressure anomalies over Central Asia, thus bringing water vapor from the tropical Indian Ocean into Central Asia (Lu et al. 2019).

AO and NAO also had important effects on EPIs in ENW. It has been shown that NAO is negatively correlated with the drought hazard in the northwest of the country. This is because the positive pattern of NAO leads to a northward shift, stronger than the mean mid-latitude westerly belt, and enhances the latitudinal moisture gradient into the drylands of Central Asia, leading to a decrease in the frequency and intensity of droughts in Northwest China (Lee and Zhang 2011). Other large-scale circulation factors, on the other hand, may modify precipitation everywhere by affecting ENSO. For example, when El Niño occurs in the negative phase of PDO, significant positive rainfall anomalies were observed over almost the entire of southern China (Li et al. 2017). In addition, the synergistic effects of multiple factors on extreme weather events were stronger than the sum of the effects of individual factors, and some studies suggest that the synergistic effects of AO and NAO may lead to a significant decrease in FD0 in the Yunnan Plateau (Avila-Diaz et al. 2021).

6 Conclusions And Future Perspectives

In this study, ten EPIs were selected to explore the spatial and temporal variations in extreme precipitation in ENW from 1961 to 2015. The geodetector model was applied to determine the main climate teleconnection factors that affect extreme precipitation. The main conclusions are as follows:

1. During 1961-2015, both CDD and CWD in ENW decreased significantly ($P<0.01$), with rates of 1.4 days/decade and 0.067 days/decade, respectively. R95p and RX5day exhibited a slight downward trend. PRCPTOT, R10, R20, R25, R99p, and RX1day showed a slight upward trend.
2. EPIs in ENW exhibited an obvious spatial heterogeneity. CDD gradually increased from the southeast to the northwest. The remaining indicators showed a roughly opposite trend, gradually decreasing from the southeast to the northwest.
3. The Hurst exponents indicated that the trend of change at some stations in the future would be consistent with that of the past. A substantial number of stations in the future may experience more severe extreme precipitation events than in the past. The frequency and intensity of extreme precipitation in the future may decrease only at a smaller number of stations.
4. The geodetector method demonstrated that large-scale circulations have a great influence on EPIs. Among the circulation factors, Nino3.4 and SO contributed more to the EPIs than others. The interaction of two teleconnection factors had a greater effect on EPIs than the sum of all individual factors and led to nonlinear enhancement.

In this study, ten EPIs in ENW and associated influencing factors were analyzed to explore the spatiotemporal pattern and associated driving mechanism of extreme precipitation. However, some limitations need to be overcome in future work:

1. Due to the high spatial and temporal heterogeneity of meteorological element distribution, the northwest region is usually divided into western and eastern parts. The number of stations used in the study was only 63 due to the topographic and climatic conditions of the eastern part of Northwest China. Although the actual observation data from the stations are more realistic and reliable, their resolution is not comparable to some remote sensing products and model data. Therefore, we

will strive to use some high-resolution satellites and model data in the follow-up study to make up for the lack of station data.

2. In this study, we initially analyzed the spatial and temporal variability and influencing factors of the annual values of the ten EPIs, while the seasonal variability characteristics of EPIs and the spatial variability and causes of seasonality were not considered for the time being. Since the impact of climate change on extreme weather events is extremely complex, seasonality is a factor that must be taken into account. Therefore, future studies will focus on seasonal variations in EPIs and related influencing factors.

Acknowledgments

The authors thank the editor and anonymous reviewers for their constructive feedback on this manuscript.

Funding

This work was supported by the Natural Science Foundation of Shandong Province (grant number: ZR2022MD077).

Author contributions

Yuhong Guo: Conceptualization, Methodology, Visualization, Writing – original draft, Writing – review and editing. Xiaodong Yan: Software, Writing – review and editing. Zhibo Gao: Methodology, Data curation, Writing – review and editing. Shuaifeng Song: Data curation, Writing – review and editing.

Declarations

Conflict of interest

The authors declare there is no conflict of interest regarding the publication of this paper.

References

Ahsan S, Bhat MS, Alam A, Farooq H, and Shiekh HA (2022) Evaluating the impact of climate change on extreme temperature and precipitation events over the Kashmir Himalaya. Clim. Dyn. 58(5): 1651-1669.https://doi.org/10.1007/s00382-021-05984-6

Ali H, Fowler HJ, and Mishra V (2018) Global Observational Evidence of Strong Linkage Between Dew Point Temperature and Precipitation Extremes. Geophys. Res. Lett. 45(22): 12,320-312,330.https://doi.org/https://doi.org/10.1029/2018GL080557

Avila-Diaz A, Bromwich DH, Wilson AB, Justino F, and Wang SH (2021) Climate Extremes across the North American Arctic in Modern Reanalyses. J. Clim. 34(7): 2385-2410.https://doi.org/10.1175/jcli-d-20-0093.1

Berg P, Haerter JO, Thejll P, Piani C, Hagemann S, and Christensen JH (2009) Seasonal characteristics of the relationship between daily precipitation intensity and surface temperature. J. Geophys.

Res.: Atmos. 114: D18102.https://doi.org/https://doi.org/10.1029/2009JD012008

Center NC. (2018). Atlas of China's Disastrous Weather and Climate (1961-2015).

Chen DD, and Dai YJ (2009) Characteristics of Northwest China Rainfall Intensity in Recent 50 Years. Chinese Journal of Atmospheric Sciences 33(5): 923-935.https://doi.org/10.3878/j.issn.1006-9895.2009.05.04

Das S (2021) Extreme rainfall estimation at ungauged locations: Information that needs to be included in low-lying monsoon climate regions like Bangladesh. J. Hydrol. 601: 126616.https://doi.org/https://doi.org/10.1016/j.jhydrol.2021.126616

Descals A, Gaveau DLA, Verger A, Sheil D, Naito D, and Peñuelas J (2022) Unprecedented fire activity above the Arctic Circle linked to rising temperatures. Science 378(6619): 532-537.https://doi.org/doi:10.1126/science.abn9768

Donat MG, Lowry AL, Alexander LV, O'Gorman PA, and Maher N (2016) More extreme precipitation in the world's dry and wet regions. Nat. Clim. Change 6(5): 508-513.https://doi.org/10.1038/nclimate2941

Fischer EM, and Knutti R (2015) Anthropogenic contribution to global occurrence of heavy-precipitation and high-temperature extremes. Nat. Clim. Change 5(6): 560-564.https://doi.org/10.1038/nclimate2617

Gao T, Wang HXJ, and Zhou TJ (2017) Changes of extreme precipitation and nonlinear influence of climate variables over monsoon region in China. Atmos. Res. 197: 379-389

Gudmundsson L, Boulange J, Do HX, Gosling SN, Grillakis MG, Koutroulis AG, Leonard M, Liu J, Müller Schmied H, Papadimitriou L, Pokhrel Y, Seneviratne SI, Satoh Y, Thiery W, Westra S, Zhang X, and Zhao F (2021) Globally observed trends in mean and extreme river flow attributed to climate change. Science 371(6534): 1159-1162.https://doi.org/doi:10.1126/science.aba3996

Guo EL, Zhang JQ, Wang YF, Quan L, Zhang RJ, Zhang F, and Zhou M (2019) Spatiotemporal variations of extreme climate events in Northeast China during 1960–2014. Ecol. Indic. 96: 669-683.https://doi.org/https://doi.org/10.1016/j.ecolind.2018.09.034

Hurst HE (1951) Long-Term Storage Capacity of Reservoirs. Transactions of the American Society of Civil Engineers 116: 770-799.

IPCC (2013): Climate change 2013: the physical science basis. Contribution of working group i to the fifth assessment report of the intergovernmental panel on climate change [Stocker, T.F., D. Qin, G.-K. Plattner, M. Tignor, S.K. Allen, J. Boschung, A. Nauels, Y. Xia, V. Bex and P.M. Midgley(eds.)]. Cambridge University Press, Cambridge, United Kingdom and New York, NY, USA, 1535.

Jiang FQ, Hu RJ, Wang SP, Zhang YW, and Tong L (2013) Trends of precipitation extremes during 1960–2008 in Xinjiang, the Northwest China. Theor. Appl. Climatol. 111(1): 133-148.https://doi.org/10.1007/s00704-012-0657-3

Kendall MG (1957) Rank Correlation Methods. British Journal of Psychology 44(1/2): 298

Kendon M, McCarthy M, Jevrejeva S, Matthews A, Sparks T, and Garforth J (2021) State of the UK Climate 2020. Int. J. Climatol. 41(S2): 1-76.https://doi.org/https://doi.org/10.1002/joc.7285

Kirschbaum D, Kapnick SB, Stanley T, and Pascale S (2020) Changes in Extreme Precipitation and Landslides Over High Mountain Asia. Geophys. Res. Lett. 47(4): e2019GL085347.https://doi.org/https://doi.org/10.1029/2019GL085347

Lee HF, and Zhang DD (2011) Relationship between NAO and drought disasters in northwestern China in the last millennium. J. Arid. Environ. 75(11): 1114-

1120.https://doi.org/https://doi.org/10.1016/j.jaridenv.2011.06.008

Lhotka O, and Kyselý J (2022) The 2021 European Heat Wave in the Context of Past Major Heat Waves. Earth Space Sci. 9(11): e2022EA002567.https://doi.org/https://doi.org/10.1029/2022EA002567

Li G, Chen JP, Wang X, Tan YK, and Jiang XH (2017) Modulation of Pacific Decadal Oscillation on the relationship of El Niño with southern China rainfall during early boreal winter. Atmos. Sci. Lett. 18(8): 336-341.https://doi.org/https://doi.org/10.1002/asl.761

Li J, Zhu ZW, and Dong WJ (2017) A new mean-extreme vector for the trends of temperature and precipitation over China during 1960–2013. Meteorol. Atmos. Phys. 129(3): 273-282.https://doi.org/10.1007/s00703-016-0464-y

Li JM, Liang J, Wang JF, Ren ZP, Yang D, Wang YP, Mu Y, Li XH, Li M, Guo YM, and Zhu J (2020) Spatiotemporal trends and ecological determinants in maternal mortality ratios in 2,205 Chinese counties, 2010–2013: A Bayesian modelling analysis. PLoS Med. 17: e1003114.https://doi.org/10.1371/journal.pmed.1003114

Li MY, Luo DH, Yao Y, and Zhong LH (2020) Large-scale atmospheric circulation control of summer extreme hot events over China. Int. J. Climatol. 40(3): 1456-1476.https://doi.org/https://doi.org/10.1002/joc.6279

Liao Z, Chen Y, Li W, and Zhai PM (2021) Growing Threats From Unprecedented Sequential Flood-Hot Extremes Across China. Geophys. Res. Lett. 48(18): e2021GL094505.https://doi.org/https://doi.org/10.1029/2021GL094505

Liu Hl, Fan Z, and Li C (2019) Comprehensive Assessment and Analysis of National Surface Meteorological Observation Stations: A Case Study of Hebei Province. Meteorological and Environmental Research v.10(04): 49-54+64

Liu R, Liu SC, Cicerone RJ, Shiu C-J, Li J, Wang JL, and Zhang YH (2015) Trends of extreme precipitation in eastern China and their possible causes. Adv. Atmos. Sci. 32(8): 1027-1037.https://doi.org/10.1007/s00376-015-5002-1

Liu Z, Gao T, Zhang W, and Luo M (2021) Implications of the Pacific meridional mode for summer precipitation extremes over China. Weather Clim. Extremes 33: 100359.https://doi.org/https://doi.org/10.1016/j.wace.2021.100359

Lu B, Jin FF, and Ren HL (2018) A Coupled Dynamic Index for ENSO Periodicity. J. Clim. 31(6): 2361-2376.https://doi.org/10.1175/jcli-d-17-0466.1

Lu B, Li HY, Wu J, Zhang TX, Liu J, Liu B, Chen Y, and Baishan J (2019) Impact of El Niño and Southern Oscillation on the summer precipitation over Northwest China. Atmos. Sci. Lett. 20(8): e928.https://doi.org/https://doi.org/10.1002/asl.928

Lu RY, Xu K, Chen RD, Chen W, Li F, and Lv CY (2023) Heat waves in summer 2022 and increasing concern regarding heat waves in general. Atmos. Oceanic Sci. Lett. 16(1): 100290.https://doi.org/https://doi.org/10.1016/j.aosl.2022.100290

Mann HB (1945) Nonparametric test against trend. Econometrica 13(3): 245-259

Mao JF, Shi XY, Ma LJ, Kaiser DP, Li QX, and Thornton PE (2010) Assessment of Reanalysis Daily Extreme Temperatures with China's Homogenized Historical Dataset during 1979–2001 Using Probability Density Functions. J. Clim. 23(24): 6605-6623.https://doi.org/10.1175/2010jcli3581.1

Marengo JA, Ambrizzi T, Barreto N, Cunha AP, Ramos AM, Skansi M, Molina Carpio J, and Salinas R (2022) The heat wave of October 2020 in central South America. Int. J. Climatol. 42(4): 2281-2298.https://doi.org/https://doi.org/10.1002/joc.7365

Ning GC, Luo M, Zhang W, Liu Z, Wang SG, and Gao T (2022) Rising risks of compound extreme heat-precipitation events in China. Int. J. Climatol. 42(11): 5785-5795.https://doi.org/https://doi.org/10.1002/joc.7561

Onali E, and Goddard J (2011) Are European equity markets efficient? New evidence from fractal analysis. International Review of Financial Analysis 20(2): 59-67

Peng YB (2018) Simulated Interannual Teleconnection Between the Summer North Atlantic Oscillation and Summer Precipitation in Eastern China During the Last Millennium. Geophys. Res. Lett. 45(15): 7741-7747.https://doi.org/https://doi.org/10.1029/2018GL078691

Perkins-Kirkpatrick SE, Stone DA, Mitchell DM, Rosier S, King AD, Lo YTE, Pastor-Paz J, Frame D, and Wehner M (2022) On the attribution of the impacts of extreme weather events to anthropogenic climate change. Environ. Res. Lett. 17(2): 24009.https://doi.org/10.1088/1748-9326/ac44c8

Qian C (2016) On trend estimation and significance testing for non-Gaussian and serially dependent data: quantifying the urbanization effect on trends in hot extremes in the megacity of Shanghai. Clim. Dyn. 47(1): 329-344.https://doi.org/10.1007/s00382-015-2838-0

Qian C, Fu CB, and Wu ZH (2011) Changes in the Amplitude of the Temperature Annual Cycle in China and Their Implication for Climate Change Research. J. Clim. 24(20): 5292-5302.https://doi.org/10.1175/jcli-d-11-00006.1

Rafatnejad A, Tavakolifar H, and Nazif S (2022) Evaluation of the climate change impact on the extreme rainfall amounts using modified method of fragments for sub-daily rainfall disaggregation. Int. J. Climatol. 42(2): 908-927.https://doi.org/https://doi.org/10.1002/joc.7280

Rastogi D, Lehner F, and Ashfaq M (2020) Revisiting Recent U.S. Heat Waves in a Warmer and More Humid Climate. Geophys. Res. Lett. 47(9): e2019GL086736.https://doi.org/https://doi.org/10.1029/2019GL086736

Rivas-Tabares DA, Saa-Requejo A, Martín-Sotoca JJ, and Tarquis AM (2021) Multiscaling NDVI Series Analysis of Rainfed Cereal in Central Spain. Remote Sens. 13(4): 568https://www.mdpi.com/2072-4292/13/4/568

Schiermeier Q (2021) Climate change made North America's deadly heatwave 150 times more likely. Nature

Schubert SD, Chang YH, Suarez MJ, and Pegion PJ (2008) ENSO and Wintertime Extreme Precipitation Events over the Contiguous United States. J. Clim. 21(1): 22-39.https://doi.org/10.1175/2007jcli1705.1

Sun J, and Zhang FQ (2017) Daily extreme precipitation and trends over China. Science China Earth Sciences 60(12): 2190-2203.https://doi.org/10.1007/s11430-016-9117-8

Sun Y, Zhang XB, Ding YH, Chen DL, Qin DH, and Zhai P (2021) Understanding human influence on climate change in China. Natl. Sci. Rev. 9(3): nwab113.https://doi.org/10.1093/nsr/nwab113

Wang CH, Zhang SN, Li KC, Zhang FM, and Yang K (2021) Change Characteristics of Precipitation in Northwest China from 1961 to 2018. Chinese Journal of Atmospheric Sciences (in Chinese) 45(4): 713-724.https://doi.org/10.3878/j.issn.1006-9895.2101.20216

Wang CH, Zhang SN, Zhang FM, Li KC, and Yang K (2021) On the Increase of Precipitation in the Northwestern China Under the Global Warming. Advances in Earth Science 36(9): 980-989.https://doi.org/10.11867/j.issn.1001-8166.2021.087

Wang JF, Zhang TL, and Fu BJ (2016) A measure of spatial stratified heterogeneity. Ecol. Indic. 67: 250-256.https://doi.org/https://doi.org/10.1016/j.ecolind.2016.02.052

Wang SS, Huang JP, He YL, and Guan YP (2014) Combined effects of the Pacific Decadal Oscillation and El Niño-Southern Oscillation on Global Land Dry–Wet Changes. Sci. Rep. 4(1): 6651.https://doi.org/10.1038/srep06651

Wang YQ, and Zhou L (2005) Observed trends in extreme precipitation events in China during 1961–2001 and the associated changes in large-scale circulation. Geophys. Res. Lett. 32(9): L09707.https://doi.org/https://doi.org/10.1029/2005GL022574

WMO. (2021). Atlas of Mortality and Economic Losses from Weather, Climate and Water Extremes (1970-2019) [EB/OL]. https://library.wmo.int/index.php?lvl=notice_display&id=21930#.Y2hoPr1Bz8

Wu ZH, and Huang NE (2009) Ensemble empirical mode decomposition: a noise-assisted data analysis method. Advances in Adaptive Data Analysis 1(1): 1-41.https://doi.org/10.1142/s1793536909000047

Yang HE, Xiaoqian ZHU, Zheng S, Wei GE, Xiaoran Z, and Mingyuan HE.

Yang Y, Ren LL, Wu MX, Wang HL, Song FF, Leung LR, Hao X, Li JD, Chen L, Li HM, Zeng LY, Zhou Y, Wang PY, Liao H, Wang J, and Zhou ZQ (2022) Abrupt emissions reductions during COVID-19 contributed to record summer rainfall in China. Nat. Commun. 13(1): 959.https://doi.org/10.1038/s41467-022-28537-9

Yao HR, Li DL, and Hui W (2017) A comparative analysis of the atmospheric circulation in summertime rainy days with different precipitation intensity in eastern Northwest China during 1981-2012. Acta Meteorologica Sinica 75(3): 384-399.https://doi.org/10.11676/qxxb2017.032

Yin L, Ping F, Mao JH, and Jin SG (2023) Analysis on Precipitation Efficiency of the “21.7” Henan Extremely Heavy Rainfall Event. Adv. Atmos. Sci. 40: 374–392.https://doi.org/10.1007/s00376-022-2054-x

Yin Q, Wang JF, Ren ZP, Li J, and Guo YM (2019) Mapping the increased minimum mortality temperatures in the context of global climate change. Nat. Commun. 10(1): 4640.https://doi.org/10.1038/s41467-019-12663-y

Yue S, and Wang CY (2004) The Mann-Kendall Test Modified by Effective Sample Size to Detect Trend in Serially Correlated Hydrological Series. Water Resour. Manage. 18(3): 201-218.https://doi.org/10.1023/B:WARM.0000043140.61082.60

Zhang GW, Zeng G, Li C, and Yang XY (2020) Impact of PDO and AMO on interdecadal variability in extreme high temperatures in North China over the most recent 40-year period. Clim. Dyn. 54(6026).https://doi.org/10.1007/s00382-020-05155-z

Zhang L, Liu Y, Zhan H, Jin M, and Liang X (2021) Influence of solar activity and EI Niño-Southern Oscillation on precipitation extremes, streamflow variability and flooding events in an arid-semiarid region of China. J. Hydrol. 601: 126630.https://doi.org/https://doi.org/10.1016/j.jhydrol.2021.126630

Zhang Q, Yang JH, Wang W, Ma PL, Lu GY, Liu XY, Yu HP, and Fang F (2020) Climatic Warming and Humidification in the Arid Region of Northwest China: Multi-Scale Characteristics and Impacts on Ecological Vegetation. J. Meteorolog. Res. 35(1): 113-127.https://doi.org/10.1007/s13351-021-0105-3

Zhang WX, and Zhou TJ (2019) Significant Increases in Extreme Precipitation and the Associations with Global Warming over the Global Land Monsoon Regions. J. Clim. 32(24): 8465-8488.https://doi.org/10.1175/jcli-d-18-0662.1

Zhang XQ, Chen YN, Fang GH, Li YP, Li Z, Wang F, and Xia ZH (2022) Observed changes in extreme precipitation over the Tienshan Mountains and associated large-scale climate teleconnections. J. Hydrol. 606: 127457.https://doi.org/https://doi.org/10.1016/j.jhydrol.2022.127457

Zhou TJ, Zhang WX, Zhang LX, Clark R, Qian C, Zhang QH, Qiu H, Jiang J, and Zhang X (2022) 2021: A Year of Unprecedented Climate Extremes in Eastern Asia, North America, and Europe. Adv. Atmos. Sci. 39(10): 1598-1607.https://doi.org/10.1007/s00376-022-2063-9

Zhu XW, Yang JL, Cui Y, and Tan ZQ (2013) Spatiotemporal Distribution and Formation Causes of Precipitation in the East of Northwest China during the Period of 1961-2009. Arid zone research 30(6): 1094-1099.http://azr.xjegi.com/CN/abstract/article_8868.shtml

778 Table 1 Station locations and data availability

Station name	Station code	Latitude (°N)	Longitude (°E)	The length of data (years)
Ejinaqi	52267	41.23	101.56	55
Dingxin	52446	40.29	99.51	55
Jinta	52447	40	98.9	27
Bayannuoergong	52495	40.46	104.58	55
Jiuquan	52533	39.76	98.48	55
Gaotai	52546	39.36	99.83	55
Alashanyouqi	52576	39.21	101.66	55
Tuole	52633	38.86	98.36	55
Yeniugou	52645	38.61	99.35	55
Zhangye	52652	38.93	100.43	55
Qilian	52657	38.18	100.3	55
Shandan	52661	38.78	101.08	55
Yongchang	52674	38.23	101.96	55
Wuwei	52679	38.08	102.91	55
Minqin	52681	38.63	103.08	55
Gangcha	52754	37.33	100.16	55
Menyuan	52765	37.45	101.61	55
Wuqiaoling	52787	37.2	102.86	55
Jingtai	52797	37.23	104.18	55
Wulan	52833	36.91	98.48	15
Dulan	52836	36.33	98.03	55
Chaka	52842	36.78	99.06	50
Gonghe	52856	36.26	100.3	55
Xining	52866	36.58	101.91	55
Guide	52868	36.36	101.36	55
Minhe	52876	36.58	102.93	55
Gaolan	52884	36.54	103.66	11
Jingyuan	52895	36.56	104.68	55
Xinghai	52943	35.79	99.66	55
Guinan	52955	35.5	100.58	17
Tongren	52974	35.5	102.08	25
Yuzhong	52983	35.86	104.15	55
Linxiadong	52984	35.58	103.18	55
Lintao	52986	35.36	103.86	55
Huajialing	52996	35.38	105	55
Mandula	53149	42.48	110.13	55
Wulatezhongqi	53336	41.66	108.8	55
Baotou	53446	40.56	109.83	55
Jilantai	53502	39.81	105.5	55
Linhe	53513	40.79	107.5	55
Huinong	53519	39.25	106.86	55

Etuokeqi	53529	39.1	107.98	55
Dongsheng	53543	39.83	109.98	55
Alashanzuoqi	53602	38.86	105.56	55
Yinchuan	53614	38.51	106.26	55
Taole	53615	38.73	106.66	55
Yulin	53646	38.28	109.41	55
Zhongwei	53704	37.53	105.16	41
Zhongning	53705	37.16	105.6	55
Yanchi	53723	37.75	107.4	55
Dingbian	53725	37.54	107.6	27
Wuqi	53738	37.08	108.25	55
Hengshan	53740	37.91	109.16	55
Suide	53754	37.6	110.06	55
Haiyuan	53806	36.56	105.9	55
Tongxin	53810	36.98	106.13	55
Guyuan	53817	35.96	106.75	55
Huanxian	53821	36.68	107.36	55
Yanan	53845	36.71	109.41	55
Xiji	53903	35.93	105.96	55
Kongtong	53915	35.54	106.66	55
Xifeng	53923	35.73	107.63	55
Luochuan	53942	35.83	109.51	55

Table 2 List of EPIs in this study

ID	Indicator name	Definition	Unit
CDD	Consecutive dry days	Maximum number of consecutive dry days (precipitation of <1 mm)	days
CWD	Consecutive wet days	Maximum number of consecutive wet days (precipitation of <1 mm)	days
PRCPTOT	Annual total wet day precipitation	Annual total from days >= 1-mm precipitation	mm
R10mm	Number of heavy precipitation days	Annual count of days when precipitation is >= 10 mm	days
R20mm	Number of very heavy precipitation days	Annual count of days when precipitation is >= 20 mm	days
R25mm	Number of extremely heavy precipitation days	Annual count of days when precipitation is >= 25 mm	days
R95p	Very wet days	Annual total precipitation of days in >95th percentile	mm
R99p	Extremely wet days	Annual precipitation of days in >99th percentile	mm
RX1day	Max 1-day precipitation amount	Annual maximum 1-day precipitation	mm
RX5day	Max 5-day precipitation amount	Annual maximum 5-day precipitation	mm

Table 3 Interaction patterns between explanatory variables

Relationship	Interaction result
$q(X1 \cap X2) < \mathrm{Min}(q(X1), q(X2))$	Weaken, nonlinear
$\mathrm{Min}(q(X1), q(X2)) < q(X1 \cap X2) < \mathrm{Max}(q(X1)), q(X2))$	Weaken, univariate
$q(X1 \cap X2) > \mathrm{Max}(q(X1), \mathrm{q}(X2))$	Enhance, bivariate
$q(X1 \cap \mathrm{X}2) = q(X1) + q(X2)$	Independent
$q(X1 \cap X2) > q(X1) + q(X2)$	Enhance, nonlinear

Table 4 Regional decadal variations of EPIs in ENW during 1961-2015

EPIs	Slope	Intercept	P_value	Trend
CDD	-1.42 days/decade	102.08 days	<0.01	Decreasing
CWD	-0.07 days/decade	4.32 days	<0.01	Decreasing
PRCPTOT	1.20 mm/decade	285.22 mm	0.37	No trend
R10	0.09 days/decade	8.08 days	0.18	No trend
R20	0.01 days/decade	2.38 days	0.72	No trend
R25	0.01 days/decade	1.42 days	0.55	No trend
R95p	-0.66 mm/decade	69.81 mm	0.28	No trend
R99p	0.04 mm/decade	20.78 mm	0.97	No trend
RX1day	0.02 mm/decade	33.00 mm	0.93	No trend
RX5day	-0.01 mm/decade	49.78 mm	1.00	No trend

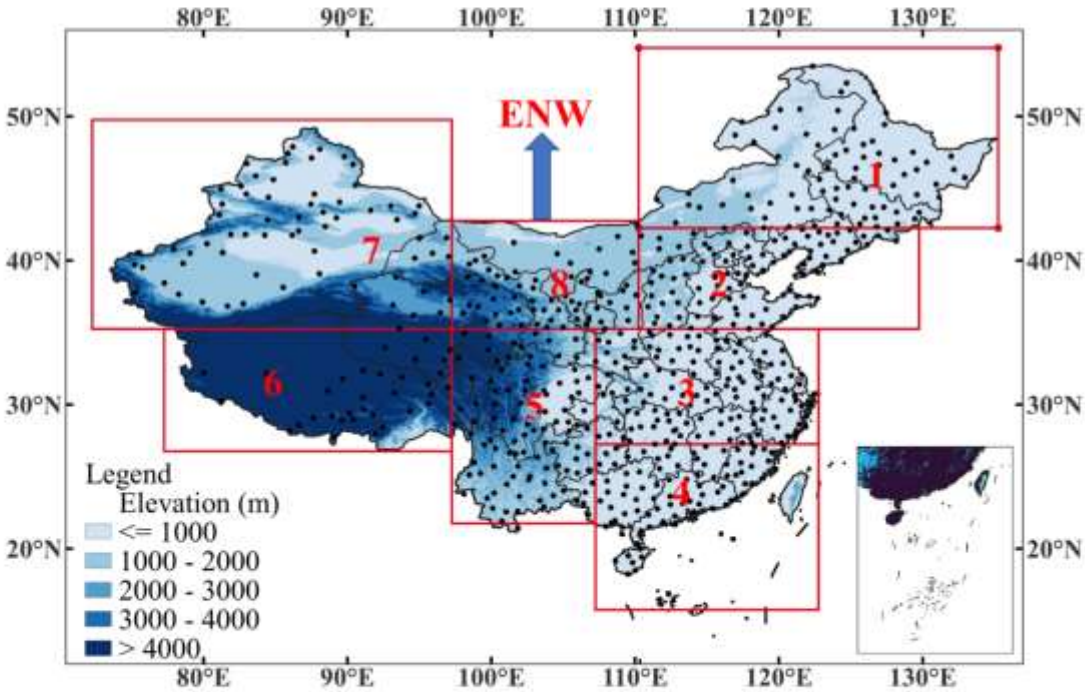

Fig. 1 Locations of weather stations in the east of Northwest China and overview of the research area (The region names represented by each number are as follows:1. Northeast (42.25-54.75°N, 110.25-135.25°E); 2. North China (35.25-42.25°N, 110.25-129.75°E); 3. Jianghuai (27.75-35.25°N, 107.25-122.75°E); 4. South China (15.75-27.25°N, 107.25-122.75°°E); 5. Southwest China (21.75-35.25°N, 97.25-107.25°E); 6. Tibetan Plateau (26.75-35.25°N, 77.25-97.25°E); 7. West of northwest China (35.25-49.75°N, 72.25-97.25°E); 8. East of northwest China (35.25-42.75°N, 97.25-110.25°E)).

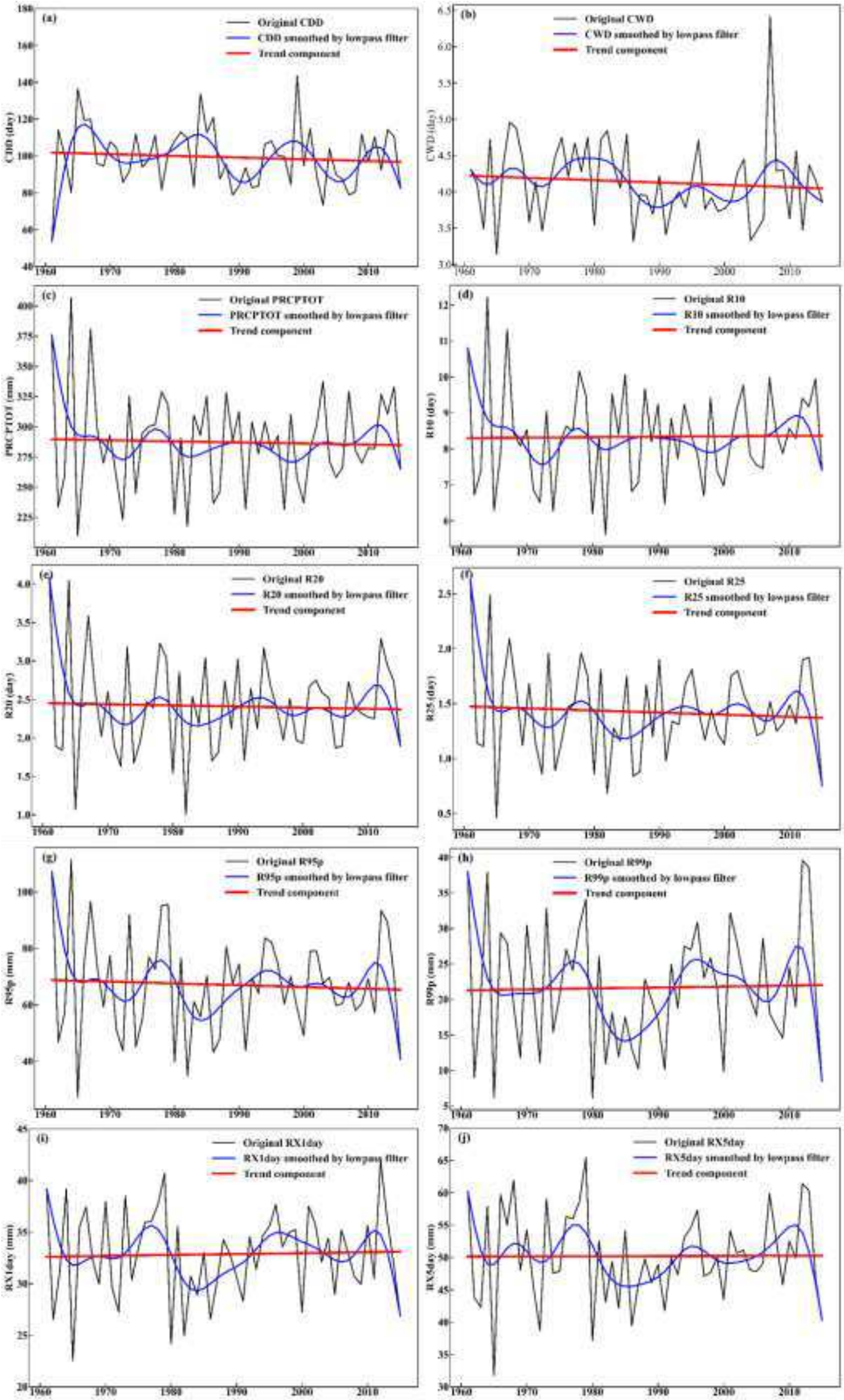

Fig. 2 Temporal changes in EPIs in ENW during 1961-2015

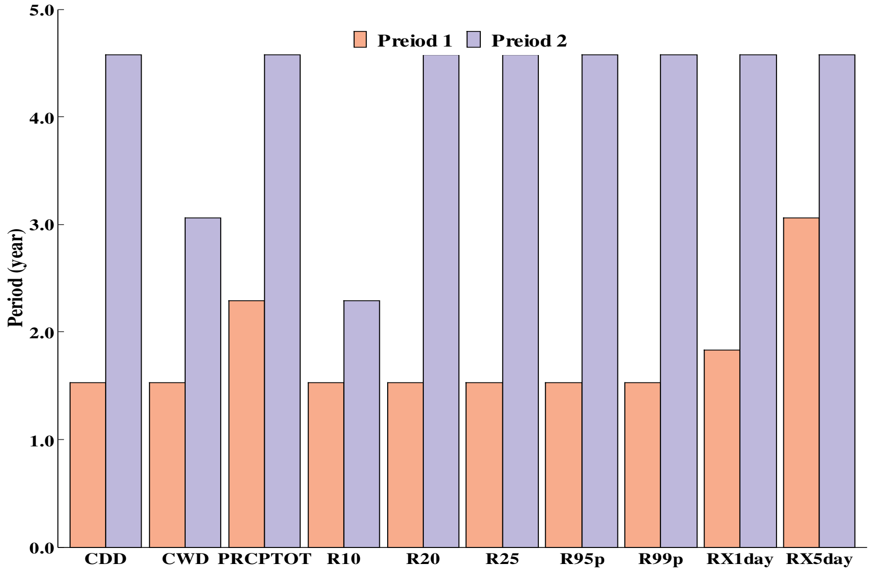

Fig. 3 Periods of EPIs in ENW during 1961-2015

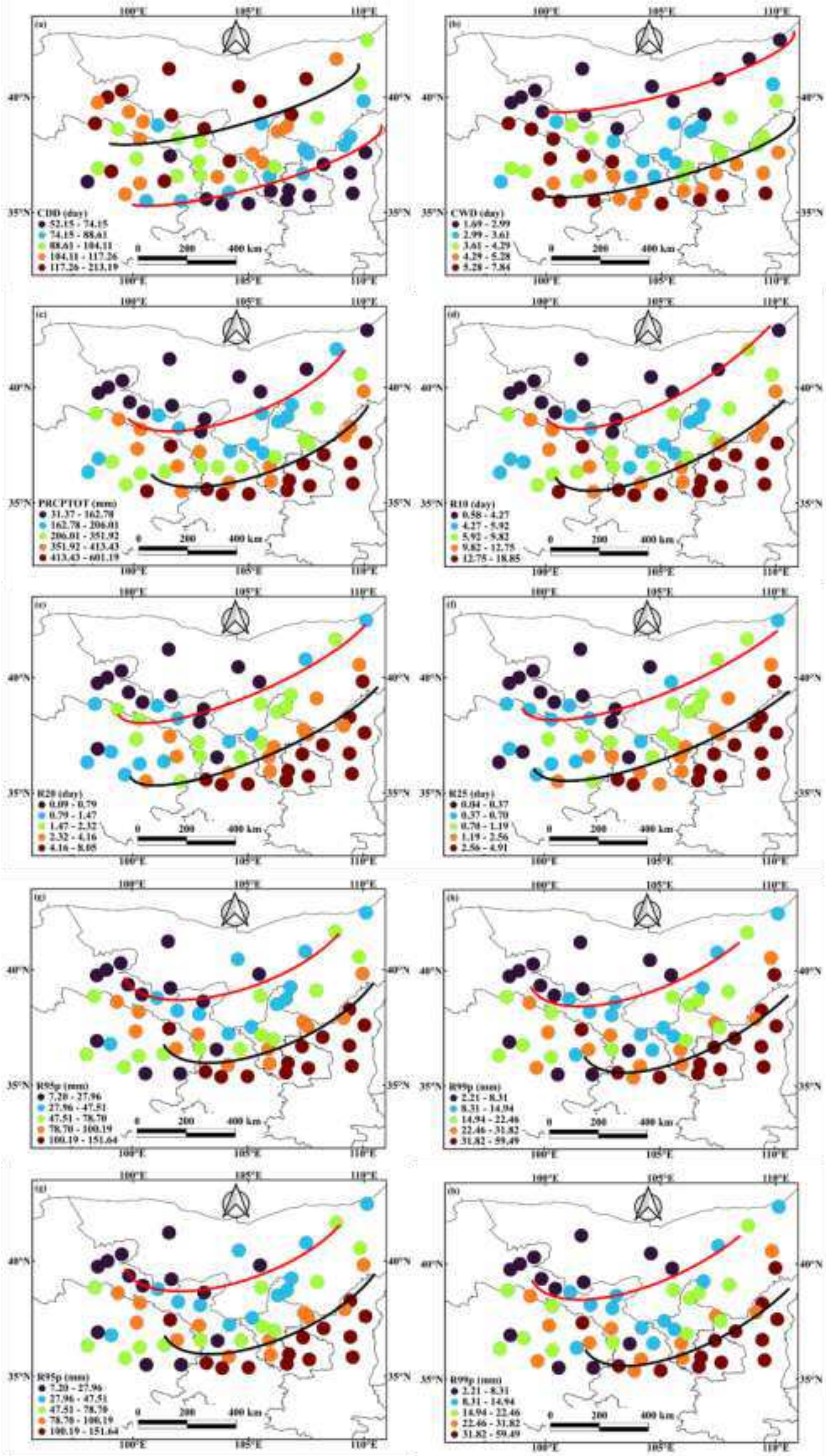

Fig. 4 Spatial distribution of EPIs in ENW during 1961-2015

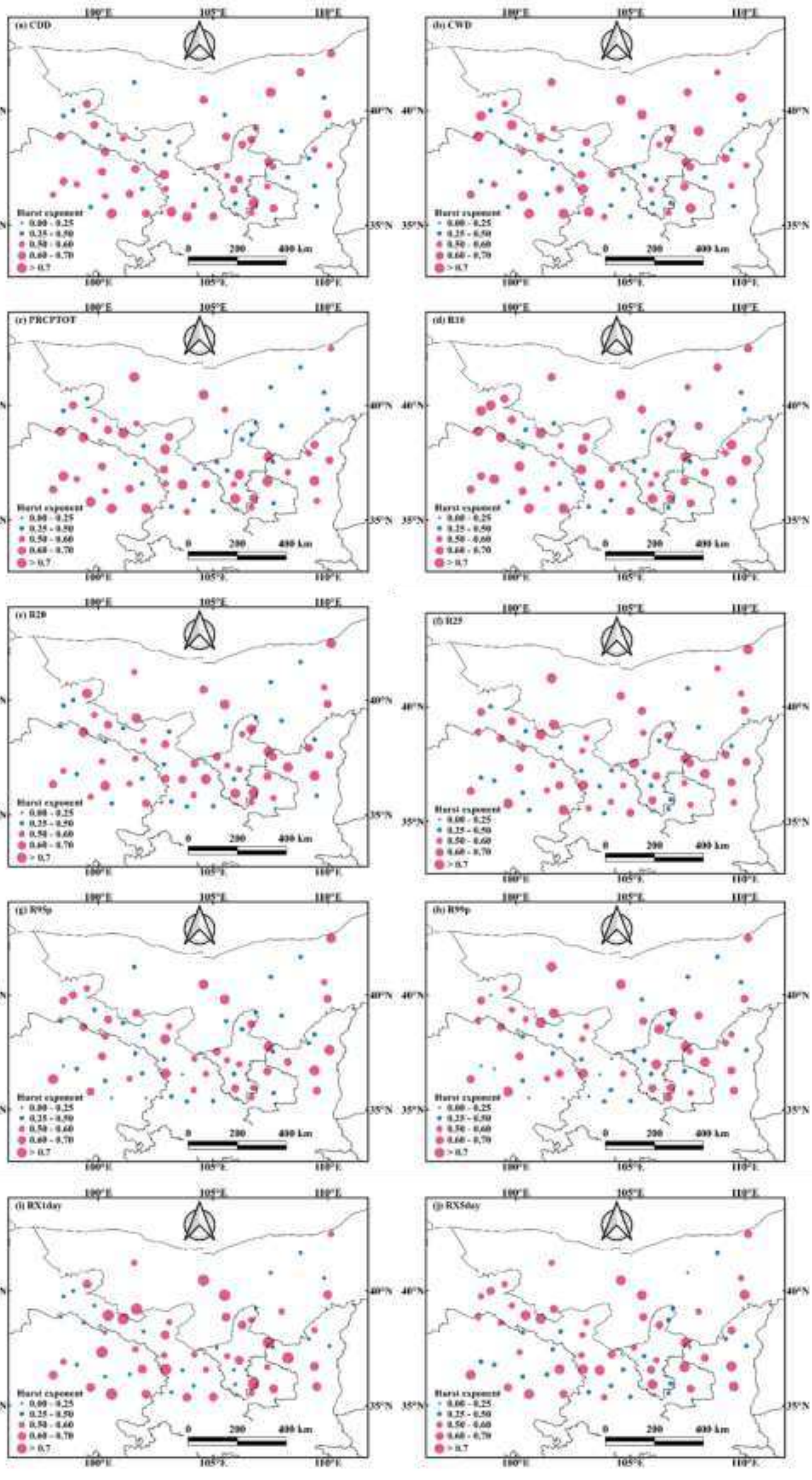

Fig. 5 Spatial distribution of Hurst values in ENW during 1961-2015

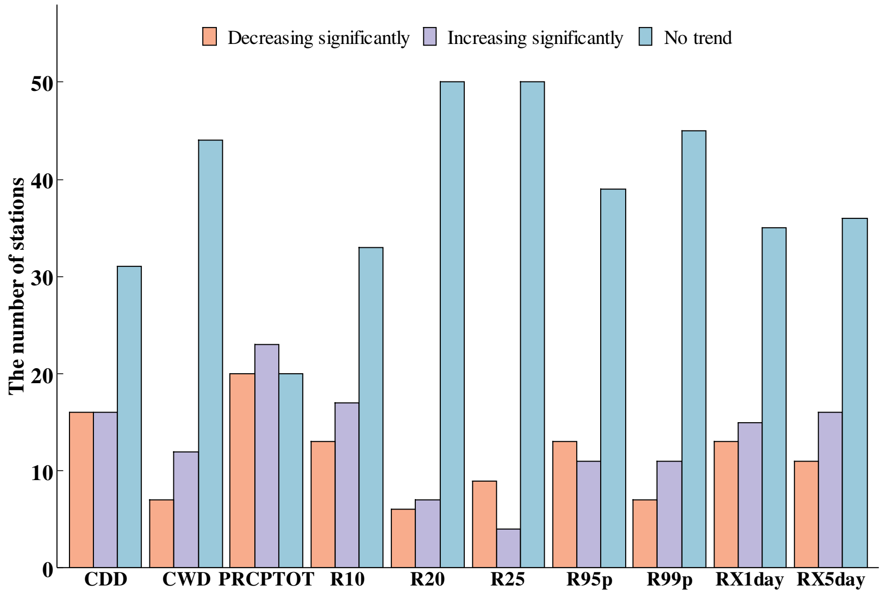

Fig. 6 The number of stations with significant trends in EPIs in ENW during 1961-2015 (Note that all the stations with trend of increasing or decreasing significantly in the figure had passed the 95% confidence test)

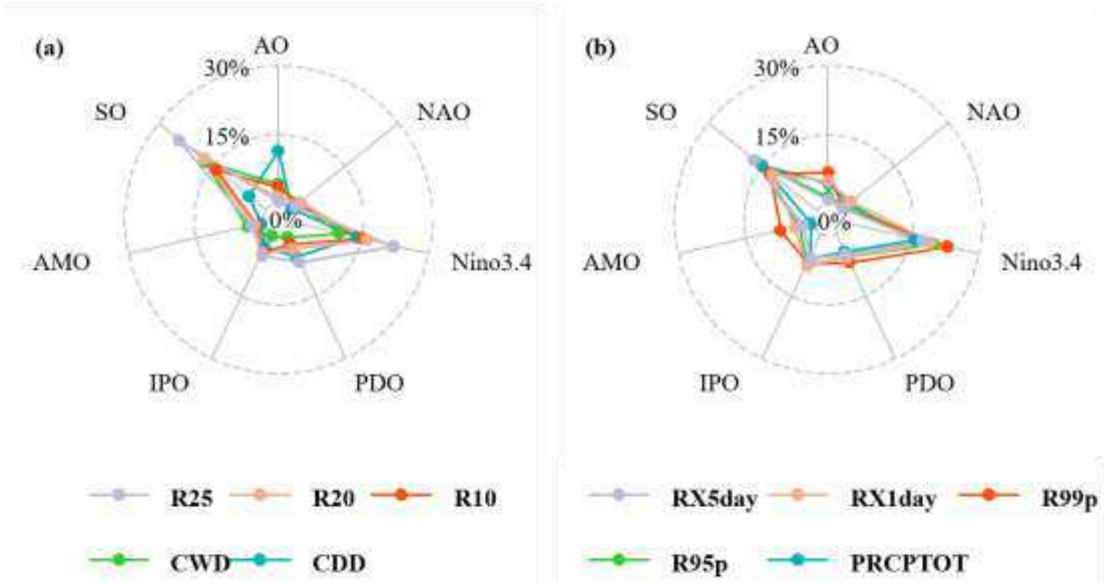

Fig. 7 Contribution of large-scale climate factors affecting EPIs in ENW

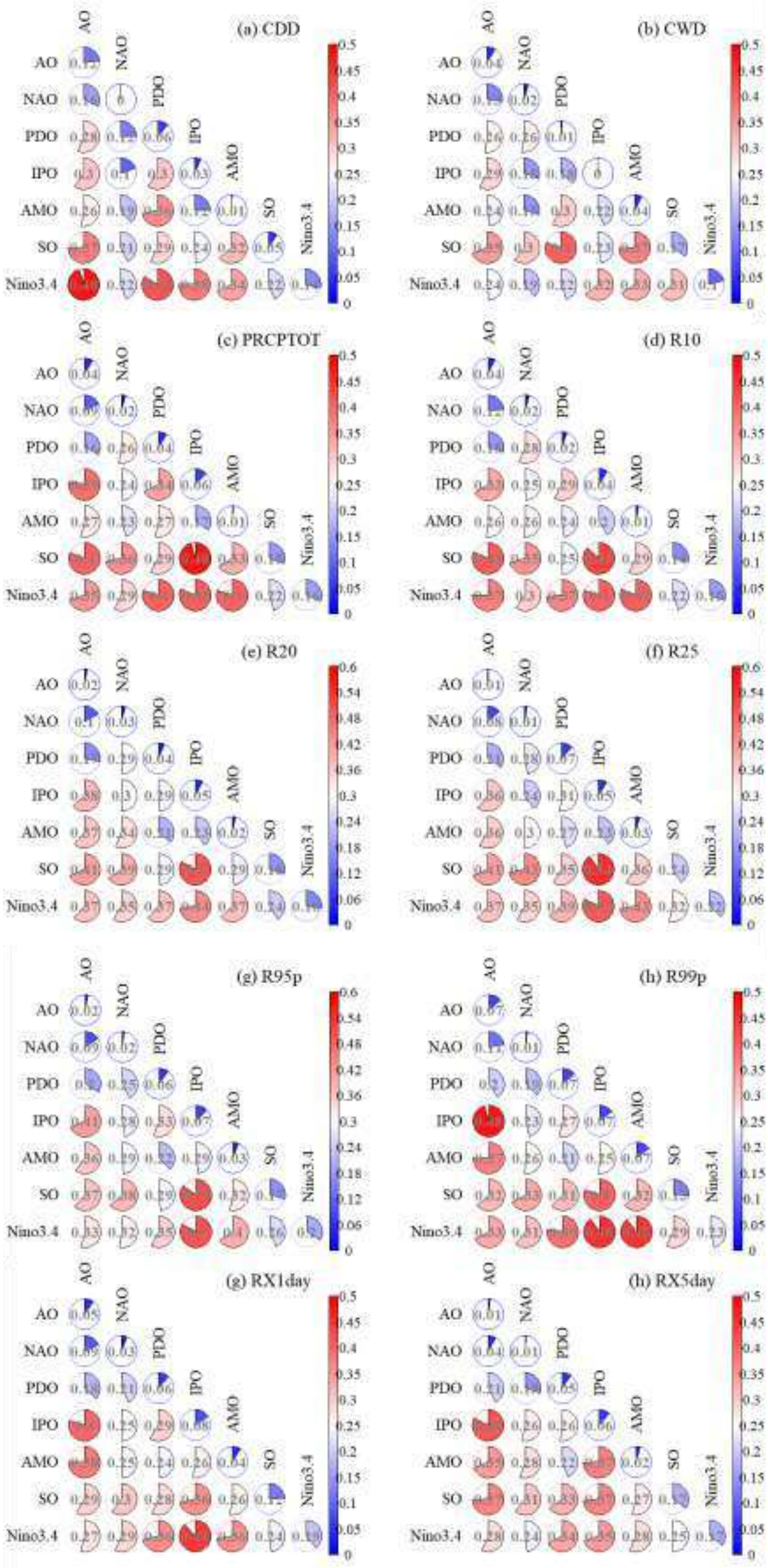

Fig. 8 Interaction detection of large-scale climate factors on EPIs in ENW